http://dx.doi.org/10.5012/bkcs.2013.34.6.1656

Structural Characterization of the Intermetallic Phase $EuZn_xIn_{4-x}$ ($x \approx 1.1$-1.2). Zn and In Site-Preferences in the $BaAl_4$ Structure-Type from Computational Analysis

Tae-Soo You,[†,‡,*] Gnu Nam,[‡] Youngjo Kim,[‡] Gregory M. Darone,[†] and Svilen Bobev[†,*]

[†]*Department of Chemistry and Biochemistry, University of Delaware, Newark, Delaware 19716, U.S.A.*
[*]*E-mail: Bobev@udel.edu*
[‡]*Department of Chemistry, Chungbuk National University, Cheongju, Chungbuk 361-763, Korea*
[*]*E-mail: tsyou@chungbuk.ac.kr*
Received February 23, 2013, Accepted March 6, 2013

The ternary phase $EuZn_xIn_{4-x}$ has been identified as the main product of reactions of Eu, Zn, and In by using the In-flux method and characterized by both powder and single-crystal X-ray diffraction. The structure belongs to the common $BaAl_4$-type (tetragonal space group $I4/mmm$, Pearson code $tI10$) with lattice parameters of $a = 4.5610(9)$ Å, $c = 12.049(3)$ Å for composition $EuZn_{1.10(12)}In_{2.90}$ and $a = 4.5463(3)$ Å, $c = 12.028(2)$ Å for composition $EuZn_{1.18(2)}In_{2.82}$, respectively. In this structure, the Eu atoms are situated at the center of 18-vertex Fedorov polyhedra made of Zn and In atoms, where the 4*d* site is preferentially occupied by In and the 4*e* site is occupied by randomly mixed Zn and In atoms. Theoretical investigations using tight-binding linear muffin-tin orbital (TB-LMTO) method provide rationale for the observed site preferences and suggest potentially wider homogeneity range than the experimentally established for $EuZn_xIn_{4-x}$ ($x \approx 1.1$).

Key Words : Crystal structure, Site-preference, Electronic structure calculations, Rare-earth intermetallics

Introduction

Polar intermetallic compounds are considered as an intermediate species between the Zintl-phase[1-3] and the typical intermetallic compounds, such as Hume-Rothery and Laves phases.[4] They provide interesting opportunities to study how the crystal structures are influenced by the electronic structures (valence electron concentrations) and the requirements for close-packing (atomic sizes of the constituting elements).[1,4,5] The polar intermetallics comprise the electropositive elements, typically members of the first three groups in the periodic table as well as rare-earth metals, combined with the electronegative elements located around Zintl boarder.[1-3] However, unlike Zintl-phases, in polar intermetallic compounds the valence electrons of the "cations" are only partially transferred to "anions",[6] and the overall "stabilization" is achieved *via* interactions between the former and the latter.[6,7] Thus, there exists no energy gap between the valence and conduction bands, but rather a local minimum in the density of states (DOS) curves is observed near the Fermi level (E_F).[8]

During our exploratory work on novel rare-earth intermetallics, by using the In-flux method,[9,10] we serendipitously obtained the new ternary phase $EuZn_xIn_{4-x}$ ($x \approx 1.1$), which crystallizes in the tetragonal $BaAl_4$-type structure.[11,12] This observation piqued our attention since the binary phase $EuIn_4$[13] has a monoclinic structure (related but not isotypic to $EuGa_4$,[12] despite the same valence electron concentration), and the partial substitution of the In atoms with the 1-electron poorer Zn atoms appears to have caused a structural transformation in $EuZn_xIn_{4-x}$ back to the $BaAl_4$-type structure. In this article, we detail the structural characterization and the structural relationships, and analyze the observed site-preference between Zn and In atoms in the polyanionic framework by comparing model electronic structures computed using the tight-biding linear muffin-tin orbital (TB-LMTO) method.

Experimental

Synthesis. Given the air-sensitivity of Eu and Li, the sample preparation process was conducted inside an argon-filled glove-box or under vacuum. The mixture of pure elements from Alfa or Aldrich (> 99.9 wt %) with the stoichiometry of 1:1:1:8 for Eu:Li:Zn:In was loaded in a 2 cm^2 alumina crucible, then flame-sealed in an evacuated fused silica ampoule to prevent oxidation at the elevated temperature. The surfaces of elemental Eu and Li were scrapped-off with scalpel blades immediately before weighing the metals. The reactions took place in a box-furnace operated at 880 °C for 10 h (ramp-rate of 50 °C/h), then slowly cooled down to 400 °C (rate of 10 °C/h). At the final stage of the process, the sealed fused-silica ampoules were taken out from the furnace and flipped-over instantaneously to remove the remaining In flux. More details about the metal-flux reaction method can be found elsewhere.[9,10]

After structure was established by single-crystal X-ray diffraction, and the composition was verified by energy-dispersive X-ray spectroscopy (EDX), another reaction was set-up with the correct stoichiometric ratio of the three elements, which successfully yielded the target product $EuZn_xIn_{4-x}$ ($x \approx 1.1$). A variation of this reaction with doubled the amount of Zn produced large crystals of $EuZn_xIn_{4-x}$ ($x \approx 1.2$). These findings are suggestive that In-flux reactions

always favor the formation of the In-rich products. Attempts to probe the homogeneity range by loading the elements with the ratio 1:2:2 for Eu:Zn:In in sealed tubes led to an inhomogeneous mixture, indicating that the reaction required to be equilibrated for longer time at lower than 450 °C temperature (at which $EuIn_4$ is in equilibrium with $EuIn_2$ according to the Eu-In phase diagram[14]) The $EuZn_xIn_{4-x}$ crystals exhibit silver color and metallic luster, indicative of them being good electrical conductors. They appeared stable in air for periods of time greater than 1 month.

Powder X-Ray Diffraction. X-ray powder diffraction patterns were collected at room temperature on a Rigaku MiniFlex powder diffractometer using Cu Kα radiation (λ = 1.54056 Å). The observed peak-positions and the peaks' relative intensities, analyzed using the JADE 6.5 software package, matched well with those calculated from the single-crystal work (Supporting Information Figure S2).

Single-Crystal X-Ray Diffraction. Single crystal X-ray diffraction data were collected at 200 K using a Bruker SMART CCD-based diffractometer with Mo $K\alpha_1$ radiation (λ = 0.71073 Å). Several crystals were checked by rapid scans before the best one was selected for further analysis. Data collection was processed with the Bruker's *SMART* software.[15] Data reduction, integration, and unit cell refinements were carried out using *SAINT*.[16] The program *SADABS*[17] was used for absorption correction based on equivalents.

Table 1. Single crystal crystallographic data and structure refinement result for $EuZn_{1.18(2)}In_{2.82}$*

Empirical formula	$EuZn_{1.18(2)}In_{2.82}$
Formula weight (g mol^{-1})	551.9
Space group, Z	*I4/mmm* (No.139), $Z = 2$
Unit cell parameters	
a (Å)	4.5463(3)
c (Å)	12.0279(18)
V (Å^3)	248.60(4)
ρ_{calcd} (g cm^{-3})	7.373
μ (cm^{-1})	307.29
θ range for data collection (°)	3.39 - 28.21
Reflections collected	933
Independent reflections	129
Data/parameters	129/10
Goodness-of-fit on F^2	1.121
Final R indices[a] ($I > 2\sigma_I$)	$R_1 = 0.0184$
	$wR_2 = 0.0446$
Final R indices[a] (all data)	$R_1 = 0.0200$
	$wR_2 = 0.0453$
Largest peak and hole (eÅ^{-3})	0.89/–1.94

[a]$R_1 = \Sigma||F_o| - |F_c||/\Sigma|F_o|$; $wR_2 = [\Sigma[w(F_o^2-F_c^2]/\Sigma[w(F_o^2)^2]]^{1/2}$, where $w = 1/[\sigma^2F_o^2+(A\cdot P)^2+B\cdot P]$, and $P = (F_o^2+2F_c^2)/3$; A and B – weight coefficients. [*] The $EuZn_{1.10(12)}In_{2.90}$ crystals appeared to be of inferior quality and the structure refinement is not presented in the tables. Selected data–diffractometer: Bruker SMART CCD, Mo-Kα radiation, λ = 0.71073 Å; θ_{max} = 29.51; crystal dimensions: 0.06 × 0.04 × 0.02 mm^3; tetragonal, *I*4/*mmm* (No. 139); a = 4.5624(5) Å; c = 12.055(3) Å; V = 250.94(6) Å^3; Z = 2; M_r = 556.9 g·mol^{-1}; $\rho_{calc.}$ = 7.370 g·cm^{-3}; μ = 304.24 cm^{-1}; 924 reflections, 130 unique; R_{int} = 0.036, R_1 = 0.055, wR_2 = 0.121; max./min. residual electron density: +5.00/ –5.44 Å^{-3}.

Table 2. Atomic coordinates, occupation factor and equivalent isotropic displacement parameters U_{eq}[a] (Å^2) for $EuZn_{1.18(2)}In_{2.82}$

Atom	Site	Occ.	x	y	z	U_{eq}
Eu	2*a*	1	0	0	0	0.0136(3)
In1	4*d*	1	1/2	0	1/4	0.0165(3)
M[b]	4*e*	0.41/0.59	0	0	0.3940(2)	0.0148(4)

[a]U_{eq} is defined as one third of the trace of the orthogonalized U_{ij} tensor. [b]Refined as a statistical mixture of In2 and Zn.

Table 3. Selected interatomic distances (Å) in $EuZn_{1.18(2)}In_{2.82}$

Atomic pair	Distance
Eu–*M*[a] (8×)	3.4583(4)
Eu–In1 (8×)	3.7695(4)
In1–*M*[a] (4×)	2.8579(7)
In1–In1 (4×)	3.2147(2)
M[a]–*M*[a]	2.550(2)

[a]Refined as a statistical mixture of In2 and Zn.

The structures were refined by full matrix least squares on F^2 using *SHELXL*,[18] refined parameters included the scale factor, the atomic positions with anisotropic displacement parameters, extinction coefficient, and occupancy factor for the mixed position.

All crystal data and refinement parameters for $EuZn_{1.18(2)}In_{2.82}$ are summarized in Table 1,* positional and equivalent isotropic displacement parameters for representative structures are listed in Table 2 and selected interatomic distances are tabulated in Table 3. CIF has also been deposited with Fachinformationszentrum Karlsruhe, 76344 Eggenstein-Leopoldshafen, Germany, (fax: (49) 7247-808-666; email: crysdata@fiz.karlsruhe.de) with depository number CSD-425858.

Magnetization Measurements. Magnetization measurements (M) were carried out in a Quantum Design PPMS in the temperature interval 5 to 290 K using an applied magnetic field (H) of 500 Oe. The measured specimen was prepared from 50 mg single-crystals, synthesized using the flux method and ground. Raw data were corrected for diamagnetic contribution from the holder and converted to molar magnetic susceptibility ($\chi_m = M/H$).

Electronic Structure Calculations. Electronic structure calculations were carried out using the tight-binding, linear muffin-tin orbital (TB-LMTO) method in the atomic sphere approximation (ASA).[19,20] Exchange and correlation were treated by the local density approximation (LDA).[21] All relativistic effects, except spin-orbit coupling, were taken into account using the scalar relativistic approximation.[22] In the atomic sphere approximation, the space is filled with overlapping Wigner-Seitz (WS) atomic spheres. The symmetry of the potential is considered spherical inside each WS sphere, and a combined correction is used to take into account the overlapping part.[23] The radii of WS sphere were obtained by requiring that the overlapping potential be the best possible approximation to the full potential, and were determined by an automatic procedure.[23] The used WS radii

are as follows: Eu = 2.399 Å, Zn = 1.369 Å, In = 1.552-1.706 Å. The basis sets included 6*s*, 6*p*, 5*d* and 4*f* orbitals for Eu; 4*s*, 4*p* and 3*d* orbitals for Zn; and 5*s*, 5*p*, and 4*d* orbitals for In. The Eu 6*p* and In 5*d* orbital were treated by the Löwdin downfolding technique,[24] and the Eu 4*f* wave-functions were treated as core states occupied by 7 electrons. The *k*-space integrations were conducted by the tetrahedron method,[25] and the self-consistent charge density was obtained using 448 irreducible *k*-points in the Brillouin zone. To interrogate the chemical bonding, crystal orbital Hamilton populations (COHP)[26] of selected interactions were also analyzed.

Results and Discussion

Crystal Structure. $EuZn_xIn_{4-x}$ ($x \approx 1.1$) crystallizes in the tetragonal $BaAl_4$-type structure[11,12] with the space group *I*4/*mmm* (*Z* = 2, Pearson symbol *tI*10). Detailed crystallographic information is tabulated in Tables 1-3, and the structure is schematically displayed in Figure 1.

The $BaAl_4$-type structure is one of the most prominent structure types observed among the intermetallic phases.[27-32] Almost all MTr_4 (*M* = alkali-earth metals or rare-earth metals; *Tr* = triels) are known to form with this structure,[33,34] however, as mentioned already, $EuIn_4$[13] and $SrIn_4$[34] are adopting quite different structures in a monoclinic *vs*. in a tetragonal crystal system, respectively. Since the crystal structure is well-known,[27-32] we will focus our attention on the observed site-preference between the Zn and In over the two available atomic sites and the structural correlation with $EuIn_4$.

The $BaAl_4$-type structure is commonly described in terms of a polyanionic framework of fused Fedorov polyhedra[36] and "cations" residing at their centers. The 18-vertex Fedorov polyhedra consists of 10 apical- (Wyckoff site 4*e*) and 8 basal-sites (Wyckoff site 4*d*) as shown in Figure 1(b).[27,28] Their 4 hexagonal and 8 rhombic faces are shared with neighboring ones, resulting in an open-framework-like 3D structure, as shown in Figure 1(c). In $EuZn_xIn_{4-x}$ ($x \approx 1.1$), the apical- (4*e*) and the basal sites (4*d*) can also be differentiated based on the Zn/In occupancies. Specifically,

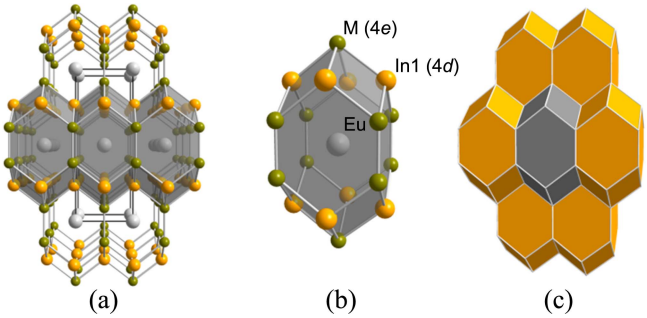

Figure 1. (a) Combined ball-and-stick and polyhedral representations of the crystal structure of the tetragonal $EuZn_xIn_{4-x}$, view down from the *b*-axis. Unit cell id outlined. (b) The 18-vertex Fedorov polyhedron centered by Eu, and (c) sharing 4 hexagonal and 8 rhombohedral faces. Color code: Eu-gray, In1-yellow, and M-green (M = Zn/In2).

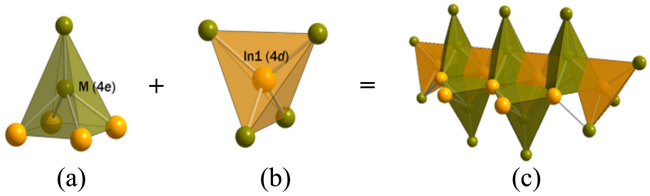

Figure 2. The two distinct anionic framework sites and their local coordination: (a) the apical-site forming the square-pyramid and (b) the basal-site constructing the distorted tetrahedron. (c) Combination of the apical- and basal-sites results in the 2D layers.

the 4*d*-sites (forming a square net) do not have any Zn, while the 4*e*-sites (forming the dimers) are statistically occupied by In and Zn. Similar preference of Zn for the apical over the basal positions has been reported for $EuZn_xAl_{4-x}$ ($1 < x < 2$),[37] as well as for $AeX^{(II)}_2X^{(III)}_2$ (Ae = Sr, Ba; $X^{(II)}$ = Mg, Zn; $X^{(III)}$ = Al, Ga) studied by Häussermann *et al*.[5] This observation cannot be rationalized based on the local coordination alone–site 4*d* displays a distorted tetrahedral environment, whereas site 4*e* has square-pyramidal coordination, as shown in Figure 2(a) and (b), respectively.[31] In fact, in many accounts, the structure is described as alternating square pyramids in the *ab*-planes (Figure 2(c)).

Given that, an in-depth analysis of the site-preference is in order. We note that we are not the first to look at this problem, it has already been reported that there are two major factors determining the distribution of the elements in the $BaAl_4$-type structures: the relative electronegativity difference and the atomic size factor of the components.[5] According to Häussermann *et al*.,[5] the more electronegative elements prefer to occupy the apical-site (4*e*) on the Fedorov polyhedron, and such compounds include $AEMg_{1.7(1)}Ga_{2.3}$ (*AE* = Sr, Ba),[5] $EuMg_xGa_{4-x}$ ($0 \le x \le 1.95$),[32] $REZn_2Al_2$ (*RE* = La, Ce),[38,39] $REZn_{1.66}Al_{2.34}$ (*RE* = Yb, Nd),[41] $AEMg_xIn_{4-x}$ (AE = Sr, $0.85 \le x \le 1.53$; *AE* = Ba, $0 \le x \le 1.79$),[31] and $AEAuIn_3$ (*AE* = Ba, Sr).[11,42] All these compounds can be considered as ternary derivatives of known binary compounds *via* the anion substitution and having valence electrons between 12 and 14. Further, Corbett has suggested that if the electronegativity difference between the framework building elements is relatively small, but their atomic sizes differ significantly, then the site-preference is more strongly influenced by the geometric factors.[31] Since the electronegativity of Zn is lower than that of In (Pauling scale: Zn = 1.68 *vs*. In = 1.78),[43] then the likely explanation for Zn to be found only on the 4*e* site in the studied $EuZn_xIn_{4-x}$ ($x \approx 1.1$) phase is the Corbett's argument–In atoms are larger than Zn atoms (r_{Zn} = 1.31 Å *vs*. r_{In} = 1.62 Å).[43] The coloring of these two available sites has been further examined by a series of theoretical calculations using the TB-LMTO-ASA method[19,20] and the details are discussed in the Electronic structure section.

Structural Relationship. The binary phase $SrAl_4$, $BaAl_4$, $EuAl_4$, $SrGa_4$, $BaGa_4$, $EuGa_4$[44] and $BaIn_4$[45] crystallize with the $BaAl_4$-type structure, while $EuIn_4$,[13] and $SrIn_4$[35] crystallize in a rare monoclinic crystal structure. Eu-Zn binary phase with stoichiometry 1:4 does not exist, therefore, the crystal structure of $EuZn_xIn_{4-x}$ ($x \approx 1.1$) can be considered as

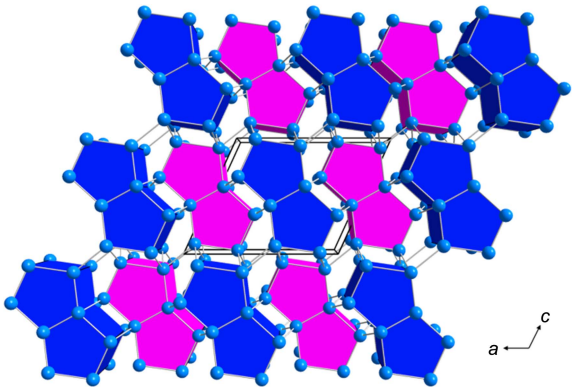

Figure 3. The crystal structure of the monoclinic $EuIn_4$ shown as a polyhedral representation with two different color codes, view down from the *b*-axis. Pairs of the magenta pentagonal-prisms are offset by a 1/2 of the *b*-lattice parameter from those of the blues. The Eu atoms embedded inside the pentagonal-prisms are not displayed for clarity.

a descendent of $EuIn_4$ and a subsequent structural transformation of the monoclinic $EuIn_4$ structure to $BaAl_4$-type structure (Figure 3), due to the partial substitution of In atoms with Zn atoms.

The crystal structure of the monoclinic $EuIn_4$[13] can be described as a 3D framework of In atoms, made of the ordered arrangement of pairs of pentagonal prisms sharing one rectangular face and propagating along the *ac*-plane (Figure 3). Each pair of pentagonal prisms is surrounded by four other neighboring pairs, which are offset by a 1/2 of the *b*-lattice parameter. In addition, those are connected to neighboring pairs *via* In–In bonds. The Eu atoms are located in the pentagonal prismatic voids within the frameworks.

According to Corbett *et al.*,[31] since the valance electron count is unchanged, the key factor determining why $EuIn_4$,[13] and $SrIn_4$[35] are not stabilized with $BaAl_4$-structure type is the size ratio between Eu (or Sr)) and In. It has been mentioned in ref. 30 that compounds made up of elements with a relatively smaller ratio between cations and anions (*e.g.* $r_{cation}/r_{anion} \leq 1.02$, such as $EuIn_4$ and $SrIn_4$) adopt the monoclinic structure, whereas those with a relatively larger ionic size ratio (*e.g.* $r_{cation}/r_{anion} \geq 1.08$, such as $SrAl_4$, $BaAl_4$, $EuAl_4$, $SrGa_4$, $BaGa_4$, $EuGa_4$ and $BaIn_4$) form with the tetragonal

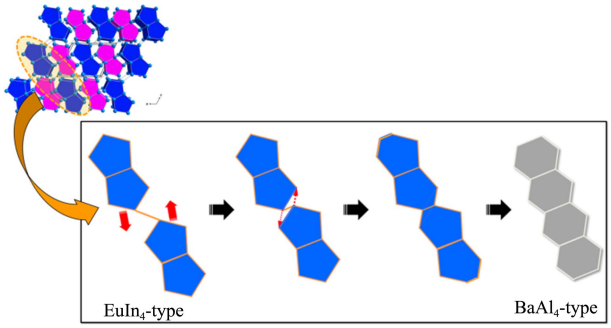

Figure 4. Schematic illustration of the structural transformation of the monoclinic $EuIn_4$-type to the tetragonal $BaAl_4$-type structure *via* bond-breaking and forming processes. See text for further details.

$BaAl_4$-type structure. Applying the same argument $EuZn_xIn_{4-x}$ is possible too: if one of the relatively larger In atom of $EuIn_4$ is substituted by a relatively smaller Zn atom (r_{In} = 1.42 Å, r_{Zn} = 1.31 Å),[43] the overall size ratio increases from 1.02 up to 1.04 ($r_{Eu}/r_{Zn\text{-}In}$ = 1.04),[46] possibly leading to the structural transformation from the monoclinic $EuIn_4$-type to the tetragonal $BaAl_4$-type structure. The earlier article mentioned that the compounds having the size ratio between 1.02 and 1.08 can crystallize in the $CaAl_4$-type structure (a distorted version of the $BaAl_4$-type), but no such distortion was observed for the Eu-Zn-In system. This could be related to the concurrent reduction on the valence electron concentration from 2.8 *e*/atom to *ca.* 2.6 *e*/atom.

The schematic illustration of the above-described structural transformation is displayed in Figure 4. As a result of the partial Zn-In substitution on the framework sites, the volume of the pentagonal prisms in the $EuIn_4$-type structure becomes smaller and insufficient to accommodate the Eu atoms. Therefore, the pentagonal prism "expands" by breaking the inner bonds of a pentagon and forming new bonds between 2 outer atoms on the opposite side. This bond-breaking and forming process transforms two pentagons into two hexagons sharing one edge together, eventually resulting in the tetragonal $BaAl_4$-type structure.

Electronic Structure and Coloring Problem. To gain a better understanding of the coloring of the apical- and the basal-sites by Zn/In and In atoms, theoretical calculations were conducted using two model structures with different Zn/In ordering, but with the same idealized composition, $EuZnIn_3$. Both structural models used lattice parameters extracted from $EuZn_{1.18(2)}In_{2.82}$ (Figure 5). For model **1**, the apical-site (4*e*), where the mixed-occupation of Zn and In was experimentally observed, was differentiated by lowering the symmetry from *I*4/*mmm* to *I*4*mm*. Then, Zn atoms were

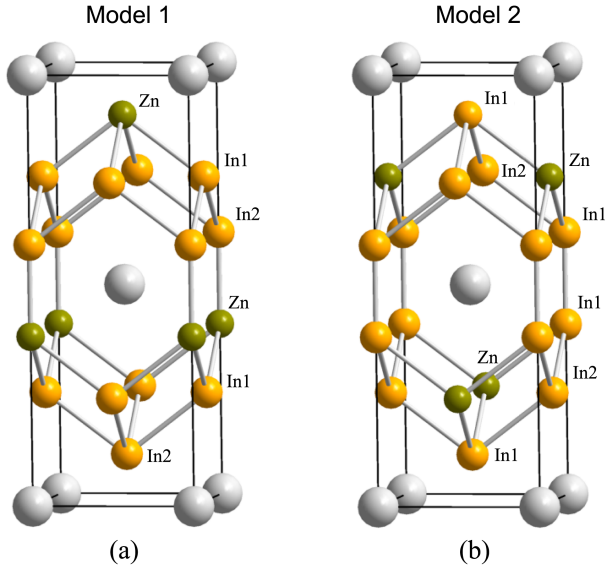

Figure 5. Two hypothetical structural models of $EuZnIn_3$ containing (a) Zn at the 50% occupancy of the 4*e* site for Model **1**, and (b) Zn at 50% occupancy of the 4*d* for Model **2**. See text for further details.

placed at the only one of two available apical sites (2*a*) as shown in Figure 5(a). For model **2**, the basal-site (4*d*) was divided into two distinct sites (2*c*, 2*d*) by lowering the symmetry to $I\bar{4}rm2$ and then Zn atoms were assigned at only one of the two basal-sites (2*d*) (Figure 5(b)), keeping the remaining framework sites occupied by In atoms. Hence, the atomic arrangement in model **1** resembles most closely that of experimentally observed structure, while model **2** exemplifies the opposite arrangement. The calculated total energies of two models confirm that the model **1** containing Zn atom at the apical-sites was energetically more favorable than model **2** by *ca*. 1.30 eV/formula unit.

To verify the observed site-preference between anionic elements, we came up with similar model structures having two different atomic arrangements. Here, we attempted to keep the identical number of valence electron concentrations, but with different size and arrangements using Ga for In. For $EuZnGa_3$, Ga with the larger electronegativity contains the smaller size than Zn. Thus, it satisfied both of two criteria simultaneously and resulted in locating Zn only at the basal site. In addition, DOS and COHP curves (Supporting Information Figure S1) are similar to those for $EuZnIn_3$. Thus, though this compound has not been reported yet, if successfully synthesized, we can expect to see the anionic site-preference just like described here.

The origin of the given total energy difference between two structural models for $EuZnIn_3$ was investigated by thorough examinations of the band-energy which exhibits the largest contribution to the structural preference. In addition, the band-energy can further be considered as a combination of the "site-energy" term and the "bond-energy" term.[26] In TB-LMTO-ASA method, the "site-energy" term is analyzed for each asymmetric site by summing the products of occupation numbers and band counts for each atomic orbital. On the other hand, the "bond-energy" term reflects the integrated COHP values of certain interatomic interactions indicating how favorable a certain interaction is.

Table 4 displays the site-energies and the bond-energies contributing to the band-energy of $EuZnIn_3$. According to the site-energies, In atoms prefer to occupy the basal-site, whereas Zn atoms prefer to be placed at the apical-sites in both models. Therefore, model **1**, where Zn is located at the one of two apical-sites (2*a*) and In at the other apical-site (2*a*) as well as the basal-sites (4*d*), is energetically the more favorable structure. Among the various bond-energies, the largest contribution comes from the anionic bonds forming the square-pyramids (Figure 2). However, the overall bond-energy term displays the smaller energy difference than the site-energy term indicating the observed site-preference is more influenced by the site-energies.

The density of states (DOS) curves calculated for the energetically favored model **1** and are displayed in Figure 6. The strong orbital mixing among Eu, Zn and In atoms is observed almost throughout the whole range (except for the

Table 4. Results of tight-binding analysis of total energy and band energy in Model **1** and Model **2**

	Model **1**		Model **2**
E_{TOT} / eV	0.000		1.302
E_{Band} / eV	0.000		8.157
Site energies / eV			
Eu	0.065		1.489
In2	−10.603		−13.980
Zn	−108.895		−106.249
In1 (2×)	−28.340		−23.819
Total	−147.773		−142.559
Bond energies / eV			
Eu-Zn (4×)	−1.859	Eu−In1 (8×)	−4.061
Eu-In2 (4×)	−2.157		
Zn-In2 (1×)	−2.017	In1−In1 (1×)	−2.293
Zn-In1 (4×)	−5.042	In1−In2 (2×)	−3.398
		Zn−In1 (2×)	−2.640
In1-In2 (4×)	−6.099	In1−In2 (2×)	−3.398
		Zn−In1 (2×)	−2.640
In1-In1 (4×)	−3.077	Zn−In2 (4×)	−1.979
Total	−20.251	Total	−20.410
Site + bond energies / eV	−168.024		−162.969
Relative total	0.000		5.055

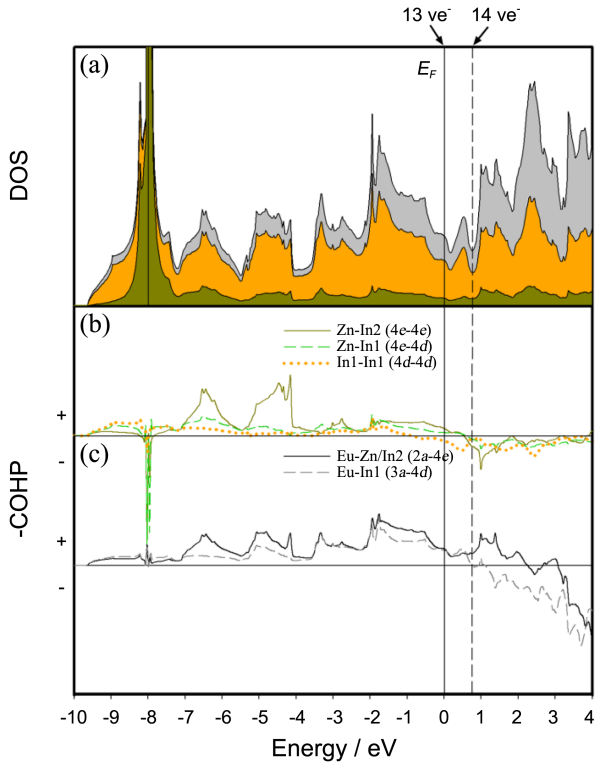

Figure 6. DOS and COHP curves calculated from Model **1**. (a) The total DOS is displayed with a solid line; partial DOS of Eu, In, and Zn are represented by the area shaded in gray, yellow, and green, respectively. E_F (solid line) is the energy reference at 0 eV. The adjacent local DOS minimum and the corresponding number of valence electrons are also shown (dashed line). COHP curves representing interatomic interactions (b) between anions, and (c) between cation and anions are also shown. The region with the "+" sign represents bonding interactions, whereas the region with the "−" sign represents antibonding interactions.

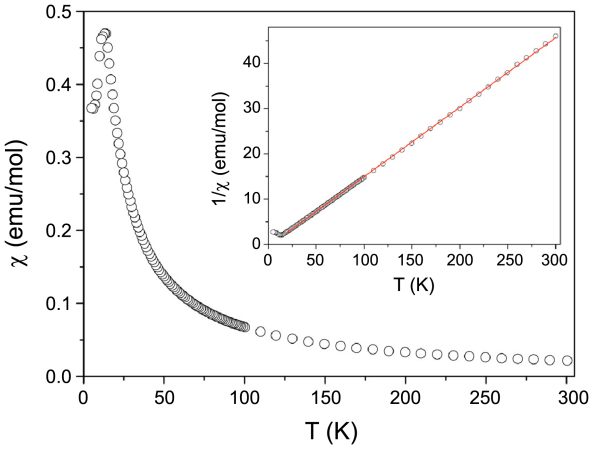

Figure 7. Magnetic susceptibility as a function of the temperature of $EuZn_{1.18(2)}In_{2.82}$. Inset: The linear fit to the inverse magnetic susceptibility as function of the temperature.

filled Zn *d*-orbitals, which are concentrated around 8 eV below E_F). This is one of the typical characteristics of polar-intermetallic compounds.[6] Within the valence region, DOS can be divided into several segments: 1) the region between –9.5 and –7.5 eV is mainly contributed by Zn 3*d* and In 5*s*; 2) the region between –7.5 and –5.7 eV is contributed by Zn 4*s* and In 5*s*; 3) the region between –5.7 and –4.0 eV is contributed by Zn 4*p* and In 5*p* (4*e*); and 4) the region between –4.0 and 0 eV is contributed by Zn 4*p* and In 5*p* (4*d*) states. E_F corresponding to 13 valence electrons (ve^-) is located just below a pseudogap observed *ca.* +0.2 eV. There exists another local minimum of DOS value around +0.8 eV corresponding to 14 ve^-. Moreover, the Zn–In2 (4*e*-4*e*) and Zn–In1 (4*e*-4*d*) COHP curves show room for additional electrons up to *ca.* +0.8 eV (Figure 6(b)). Although the In1–In1 (4*d*-4*d*) COHP curve shows the antibonding character above E_F, this character can be compensated by favorable interactions of Zn–In1/In2, Eu–Zn/In2 and Eu–In1 (Figure 6(b), (c)).

Therefore, if we apply the rigid band concept,[48] the $BaAl_4$-type structure is expected to remain electronically stable up to 14 valence electrons (per formula init) as known for this bonding arrangement.[31,32] These results support the experimental evidence for a small phase-width in $EuZn_xIn_{4-x}$, but this theoretical approach cannot explain the "driving force" for the structural transformation from the monoclinic $EuIn_4$ to the tetragonal $EuZn_{1.18(2)}In_{2.82}$ structure, which we earlier attributed to optimization of the close-packing.

Magnetism. Magnetic susceptibility of $EuZn_xIn_{4-x}$ ($x \approx 1.1$) as a function of the temperature is shown in Figure 7. The data fits well to the Curie–Weiss law $\chi = C/(T - \theta_{CW})$, where C is the Curie constant ($C = N_A\mu_{eff}^2/3k_B$) and q_{CW} is the Weiss temperature. The calculated effective magnetic moment is $\mu_{eff} = 7.58\ \mu_B$ and $\theta_{CW} = 2$ K. The calculated effective magnetic moment for the europium is slightly lower than the expected Eu^{2+} free-ion moment (7.94 μ_B according to the Hund's rules[49]), which is most likely due to small amounts of residual In metal in the sample (not fully removed flux). There is a clearly defined maximum in χ(T) below 20 K, which is suggestive of an antiferromagnetic ordering with Neel temperature *ca.* 16 K. However, the Weiss temperature θ_{CW} is slightly positive, which is an indication of ferromagnetic correlations. Both the ordering temperature and effective magnetic moment reported herein are in good agreement with earlier results for $EuGa_4$ ($T_N = 15$ K, $\theta_{CW} = 3$ K).[12]

Conclusion

The new phase $EuZn_xIn_{4-x}$ ($x \approx 1.1$) has been synthesized and structurally characterized. This phase adopts the $BaAl_4$-type structure, even though the "parent" $EuIn_4$ phase crystallizes with a different monoclinic structure. The experimental observation that the Zn atoms are located preferentially at the apical-site contradicts well-known "electronic" arguments, which would not place the less electronegative element at this site of the $BaAl_4$-type structure (as exemplified by $ThCr_2Si_2$ and the numerous ternary derivatives). We speculated that the need for close-packing overrides the electronic requirements and allows $EuZn_xIn_{4-x}$ ($x \approx 1.1$) to be stabilized with the $BaAl_4$-type structure with less than the optimal number of valence electrons. A circumstantial evidence in support of this thinking is the fact that the isostructural $EuZn_xAl_{4-x}$ ($1 < x < 2$)[36] has larger stoichiometry breadth and electron count well into the electron deficient range (12 valence electrons for the composition $EuZn_xAl_{4-x}$ ($x \approx 2$)). All of the above is a testament that the bonding in these simple materials is not yet fully understood and calls for further exploratory work, possibly involving different dopant elements.

Acknowledgments. Svilen Bobev acknowledges financial support from the National Science Foundation through a grant DMR-0743916 (CAREER). This research was supported by Basic Science Research Program through the National Research Foundation of Korea (NRF) funded by the Ministry of Education, Science and Technology (grant number 2012010941).

Supporting Information. Crystallographic data can be obtained free of charge from FIZ, D-76344, Eggenstein-Leopoldshafen, Germany, E-mail: crysdata@fiz-karlsruhe.de. DOS and various COHP curves of $EuZnGa_3$ are provided. Powder X-ray diffraction pattern of title compound is also shown.

References

1. You, T.-S.; Grin, Y.; Miller, G. J. *Inorg. Chem.* **2007**, *46*, 8801.
2. He, H.; Stearrett, R. Nowak, E. R.; Bobev, S. *Inorg. Chem.* **2010**, *49*, 7935.
3. Wang, J.; Xia, S.-Q.; Tao, X.-T. *Inorg. Chem.* **2012**, *51*, 5771.
4. Westbrook, J. H.; Fleischer, R. L. *Intermetallic Compounds: Principle and Practice*, Wiley: New York, 1995.
5. Misra, S.; Miller, G. J. *J. Am. Chem. Soc.* **2008**, *130*, 13900.
6. Klem, M. T.; Vaughey, J. T.; Harp, J. G.; Corbett, J. D. *Inorg.*

Chem. **2001**, *40*, 7020.
7. Gout, D.; Barker, T. J.; Gourdon, O.; Miller, G. J. *Chem*. *Mater*. **2005**, *17*, 3661.
8. Miller, G. J.; Lee, C.-S.; Choe, W. In *Highlights in Inorganic Chemistry*; Meyer, G., Ed., Wiley-VCH: Heidelberg, Germany, 2002; p 21.
9. You, T.-S.; Tobash, P. H.; Bobev, S. *Inorg*. *Chem*. **2010**, *49*, 1773.
10. Kanatzidis, M. G.; Pöttgen, R.; Jeitschko, W. *Angew. Chem*. *Int. Ed.* **2005**, *44*, 6996.
11. Liu, S.; Corbett, J. D. *Inorg*. *Chem*. **2004**, *43*, 4988.
12. Bobev, S.; Bauer, E. D.; Thomson, J. D.; Sarrao, J. L. *J. Magn*. *Magn*. *Mater*. **2004**, *277*, 236.
13. Dai, J.-C.; Gupta, S.; Corbett, J. D. *Inorg*. *Chem*. **2011**, *50*(1), 238.
14. Yatsenko, S. P.; Semyannikov, A. A.; Shakarov, H. O.; Fedorova, E. G. *J. Less-Common Met*. **1983**, *90*, 95.
15. Bruker, SMART, Bruker AXS Inc., Madison, Wisconsin, USA, 2002.
16. Bruker, SAINT, Bruker AXS Inc., Madison, Wisconsin, USA, 2002.
17. Sheldrick, G. M. SADABS, University of Göttingen, Germany, 2003.
18. Sheldrick, G. M. SHELXTL, University of Göttingen, Germany, 2001.
19. Andersen, O. K. *Phys*. *Rev.* **1986**, *B 34*, 2439.
20. Jepsen, O.; Burkhardt, A.; Andersen, O. K. *The TB-LMTO-ASA Program*, version 4.7, Max-Planck-Institut für Festkörperforschung, Stuttgart, Germany, 1999.
21. Andersen, O. K.; Jepsen, O. *Phys*. *Rev. Lett*. **1984**, *53*, 2571.
22. Andersen, O. K.; Jepsen, O.; Glötzel, D.; Bassani, F.; Fumi, F.; Tosi, M., Eds.; *Highlights of Condensed Matter Theory*; North-Holland, Lambrecht, W. R. L., New York, 1985.
23. Jepsen, O.; Anderson, O. K. *Z. Phys*. *Rev.* **1995**, *B 97*, 35.
24. Dronskowski, R.; Blöchl, P. E. *J. Phys*. *Chem*. **1993**, *97*, 8617.
25. Blöchl, P. E.; Jepsen, O.; Anderson, O. K. *Phys. Rev.* **1994**, *B 49*, 16223.
26. Miller, G. J. *Eur. J. Inorg. Chem.* **1998**, *5*, 523.
27. Zheng, C.; Hoffmann, R. *Z. Naturforsch*. **1986**, *41B*, 292.
28. Burdett, J. K.; Miller, G. J. *Chem*. *Mater*. **1990**, *2*, 12.
29. Szytula, A.; Leciejewicz, J. *Handbook of Crystal Structures and Magnetic Properties of Rare Earth Intermetallics*; CRC Press: Boca Raton, FL 1994.
30. Fedorchuk, A.; Prots, Yu.; Grin, Yu. *Z. Kristallogr*. **2005**, *NCS 220*, 317.
31. Li, B.; Corbett, J. D. *Inorg*. *Chem*. **2007**, *46*, 8812.
32. You, T.-S.; Miller, G. J. *Z. Anorg*. *Allg*. *Chem*. **2008**, *634*, 845.
33. Pearson, W. B. *J. Less-Common Met*. **1985**, *L3*, 109.
34. Pearson, W. B. *J. Solid State Chem*. **1985**, *56*, 278.
35. Seo, D.-K.; Corbett, J. D. *J. Am. Chem. Soc*. **2000**, *122*, 9621.
36. von Fedorov, J. S. *Z. Kristallogr*. **1904**, *38*, 321.
37. Häussermann, U.; Amerioun, S.; Eriksson, L.; Lee, C.-S.; Miller, G. J. *J. Am*. *Chem*. *Soc*. **2002**, *124*, 4371.
38. Verbovytskyy, Yu.; Kaczorowski, D.; Goncalves, A. P. *Intermetallics* **2011**, *19*, 613.
39. Ikromov, A. Z.; Ganiev, I. N.; Kinzhibalo, V. V. *Dokl*. *Akad*. *Nauk Tadzh*. *SSR*. **1990**, *33*, 173.
40. Cordier, G.; Czech, E.; Schäfer, H.; Woll, P. *J. Less-Common Met*. **1985**, *110*, 327.
41. Stel'makhovych, B.; Stel'makhovych, O.; Kuz'ma, Yu. *J. Alloys Compd*. **2005**, *397*, 115.
42. Dai, J.-C.; Corbett, J. D. *Inorg*. *Chem*. **2007**, *46*, 4592.
43. Pauling, L. *The Nature of the Chemical Bond*, 3rd ed.; Cornell University Press: Ithaca, NY, 1960; p 403.
44. Villars, P.; Calvert, L. D. *Pearson's Handbook of Crystallographic Data for Intermetallic Phases*, 2nd ed.; American Society of Metals: Park, OH, 1991.
45. Wendorff, M.; Röhr, C. *Z. Anorg*. *Allg*. *Chem*. **2005**, *631*, 338.
46. To obtain these ionic ratios, we used the values exploited by Corbett *et al.* Therefore, Shannon's radii [46] were used for cations, and radii from the elemental structures [42] were exploited for anions.
47. Shannon, R. *D. Acta Crystallogr*. **1976**, *A32*, 751.
48. Tkachuk, A. V.; Mar, A. *J. Solid State Chem*. **2007**, *180*, 2298.
49. Kittel, C. *Introduction to Solid-State Physics*, 7th ed.; John Wiley & Sons, Inc.: 1996.